UDC 539.4

Study on the Compression Moulding of Intercrossed Pre-Preg Glass Fiber-Reinforced Plastic

J. W. Kim

Department of Mechanical System Engineering, Chosun University, Republic of Korea

jinu763@chosun.ac.kr

In this paper, pre-preg intercrossed GFRP composite is cut in the square and undergone through hot compression moulding. During this process, flow front of actual sample and simulation results with finite element method (FEM) is compared. Pre-preg intercrossed GFRP composite is made of stacking plain weaved pre-preg, and material cannot be slipped by the entanglement between fibers. Based on the assumption of the significant influence of friction, $\alpha = 100$ of slip parameter is used in FEM flow analysis according to the Galerkin method, which is well matched to experimental results.

Keywords: glass fiber-reinforced plastic, compression moulding, finite element method, flow front, Galerkin method, slip parameter

Introduction. Glass fiber-reinforced plastic (GFRP) composites are anisotropic materials that have different flow characteristics in longitudinal and transverse direction of the fiber. Anisotropy of viscosity and friction between mould and material is considered to conduct FEM analysis. This methodology can have the benefits of cost reduction from repeated test, saving material development lead time, prevention of weld line, determination of moulding condition, analysis on flow characteristics and physical properties. Therefore, to identify the flow state of materials within mould during hot compression moulding of GFRP composite, slip between mould and material interface and slip parameter needs to be confirmed [1–7].

Interface at GFRP composite is an important factor that can influence mechanical properties of final composite materials. Intrinsic physical/chemical/mechanical properties of reinforcing fiber and resin are significantly varied, and properties of the interface will dominate the mechanical performance of composites. For example, if interface strength is low, the composite material will be determined by low interface strength, and reinforcement with high strength and high elasticity cannot ensure sufficiently and expected performance level. If interface strength is too high, resistance for crack propagation becomes low, and fracture toughness is dropped. Study up to now handles material under moulding process as pseudo plastic fluid, and there is no slip at the interface between mould and material for flow analysis. However, as the viscosity of material increases, the slip will occur at the interface [8–14].

The orientation of reinforcing fiber is random in composite, and it is treated as isotropic Newtonian fluid for analysis in the two-dimensional plate. These methods have the limitation for FEA on high anisotropy considering slip at the mould-material surface. In this study, pre-preg intercrossed GFRP composite is cut out in the square, and pressed via hot compression flow moulding. Experimental results and FEM analysis on flow front are compared and reviewed.

1. **Governing Equation**. To derive flow front of GFRP composite, two-dimensional hot compression flow moulding in the arbitrary plane as shown in Fig. 1 is considered. According to the non-compressive condition, continuity equation can be denoted as follows:

$$\frac{\partial u}{\partial x}+\frac{\partial v}{\partial y}+\frac{\partial w}{\partial z}=0, \tag{1}$$

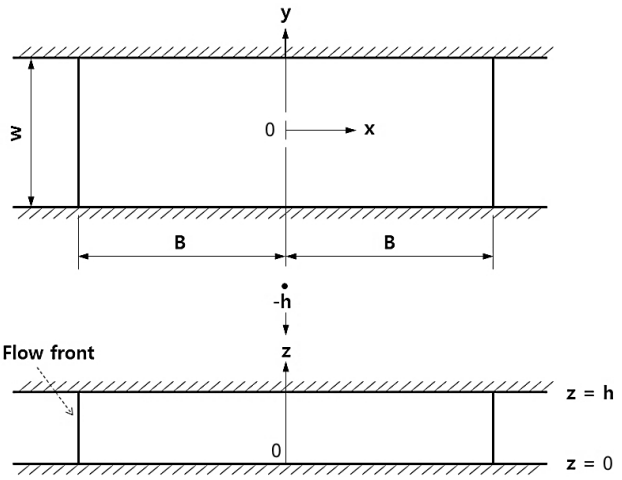

Fig. 1. Coordinate systems using derivation of governing equations.

where u, v, and w is flow rate at x, y, and z direction, respectively. Value of $\dot{h}$ is compression rate, and flow rate component at mould surface, $z = w = \pm \dot{h}/2$. Therefore, w can be denoted as follows:

$$w = \frac{\dot{h}}{h^2}. \tag{2}$$

From Eqs. (1) and (2), continuity equation can be derived as below:

$$\frac{\partial u}{\partial x} + \frac{\partial v}{\partial y} + \frac{\dot{h}}{h} = 0, \tag{3}$$

$$-\frac{\partial p}{\partial x} + \mu_x \left\{ \left(\frac{\partial^2 u}{\partial x^2} + \frac{\partial^2 u}{\partial y^2} \right) + \frac{1}{3} \left(\frac{\partial^2 u}{\partial x^2} + A \frac{\partial^2 v}{\partial x \partial y} \right) \right\} = 0, \tag{4}$$

$$-\frac{\partial p}{\partial x} + \mu_x \left\{ A \left(\frac{\partial^2 v}{\partial x^2} + \frac{\partial^2 v}{\partial y^2} \right) + \frac{1}{3} \left(\frac{\partial^2 u}{\partial x \partial y} + A \frac{\partial^2 v}{\partial y^2} \right) \right\} = 0. \tag{5}$$

For Eqs. (4) and (5), A is viscosity ratio (μ_y / μ_x) in x and y direction.

With considering slip term at mould-material interface into Eqs. (3), (4), and (5) and substituting boundary condition, the complete solution can be derived. However, this equation can be used only in the dimensionless form. Therefore, dimensionless parameters are defined as follows:

$$\bar{x} = \frac{x}{L}, \quad \bar{y} = \frac{y}{L}, \quad \bar{u} = \frac{d\bar{x}}{d\bar{t}}, \quad \bar{u} = \frac{d\bar{y}}{d\bar{t}}, \quad \bar{P} = -\frac{Ph}{2K_H \dot{h} L^2},$$

$$\frac{dx}{d\bar{x}} = L, \quad \frac{\partial \bar{x}}{\partial x} = \frac{1}{L}, \quad \frac{dy}{d\bar{y}} = L, \quad \frac{d\bar{y}}{dy} = \frac{1}{L}, \quad \frac{\partial \bar{t}}{\partial t} = -\frac{\dot{h}}{h}, \tag{6}$$

$$\bar{t} = \log\left(\frac{h_0}{h(t)} \right), \quad \alpha = \frac{\mu_x}{2K_H L^2},$$

where K_H is fluid friction coefficient, and the continuity equation (3), equations of motion (4) and (5) can be denoted as dimensionless constitutive equations:

$$\frac{\partial \bar{u}}{\partial \bar{x}} + \frac{\partial \bar{v}}{\partial \bar{y}} + 1 = 0, \tag{7}$$

$$-\frac{\partial \bar{p}}{\partial \bar{x}} + \alpha \left\{ \left(\frac{\partial^2 \bar{u}}{\partial \bar{x}^2} + \frac{\partial^2 \bar{u}}{\partial \bar{y}^2} \right) + \frac{1}{3} \left(\frac{\partial^2 \bar{u}}{\partial \bar{x}^2} + A \frac{\partial^2 \bar{v}}{\partial \bar{x} \partial \bar{y}} \right) \right\} + \bar{u} = 0, \tag{8}$$

$$-\frac{\partial \bar{p}}{\partial \bar{x}} + \alpha \left\{ A \left(\frac{\partial^2 \bar{v}}{\partial \bar{x}^2} + \frac{\partial^2 \bar{v}}{\partial \bar{y}^2} \right) + \frac{1}{3} \left(\frac{\partial^2 \bar{u}}{\partial \bar{x} \partial \bar{y}} + A \frac{\partial^2 \bar{v}}{\partial \bar{y}^2} \right) \right\} + \bar{v} = 0. \tag{9}$$

From Eqs. (8) and (9), dimensionless constant, α, which governs slip at the mould-material interface, is determined by flow rate field, and its range is between $0 \sim \infty$. If $\alpha = 0$, simple expanding flow occurs with the same flow front as the one predicted by the generalized Hele-Shaw (GHS) model. As α increases, there is no slip at the interface, and initial shape during moulding can be maintained during the flow. That is, if friction is high ($K_H = \infty$), there is no slip ($\alpha = 0$). If friction is low ($K_H = 0$), slipping happens all the time ($\alpha = \infty$), and flow front will maintain the initial charging state.

Meanwhile, u, v and $\bar{u}$, $\bar{v}$ has the following relationship from Eq. (6):

$$u = \frac{\dot{h}}{h} L\bar{u}, \qquad v = \frac{\dot{h}}{h} L\bar{v}. \tag{10}$$

2. **Finite Element Formulation**. To define flow rate distribution of GFRP composites in mould, solution from governing equations of (7), (8), and (9) needs to be resolved using boundary element method or numerical analysis on FEM. In this study, finite element method is used to derive the solution, and given governing equations are converted to the weighted residual equation using the Galerkin approach. Using FEM, it is converted to the separated equations, the coefficient of governing equation, $\bar{u}$, $\bar{v}$, and $\bar{p}$ is determined; $\bar{u}$, $\bar{v}$ is calculated from u, v.

Weighting function, P^*, is multiplied by both variants of Eq. (6) in the dimensionless continuity equation, and can be integrated for the arbitrary area V:

$$\int_V^0 P^* (\bar{u}_{,x} + \bar{v}_{,y} + 1) dxdy = 0. \tag{11}$$

For steady flow of incompressible viscous fluid, interpolation function of flow rate and pressure needs to avoid duplication into simultaneous equation in total system. Interpolation function and weighted function should be 2nd order for flow rate and 1st order equation for pressure. The element was a secondary trigonal one, and the corresponding interpolation function for flow rate and pressure is the following:

$$u = \Phi_\alpha (x, y) u_\alpha, \qquad v = \Phi_\alpha (x, y) v_\alpha, \qquad \alpha = 1 \sim 6, \tag{12}$$

$$P = \Psi_\alpha (x, y) P_\lambda, \qquad \lambda = 1 \sim 3. \tag{13}$$

The weighted function is as follows:

$$u^* = \Phi_\alpha(x,\ y)u_\alpha^*, \qquad v^* = \Phi_\alpha(x,\ y)v_\alpha^*, \qquad \alpha = 1 \sim 6, \tag{14}$$

$$P^* = \Psi_\alpha(x,\ y)P_\lambda^*, \qquad \lambda = 1 \sim 3. \tag{15}$$

By substituting Eqs. (12)–(15) into continuity equation (11), it is summarized as

$$P_\lambda^* \left[\int_V^0 (\Psi_\lambda \Phi_{\lambda,x})dxdyu_\beta + \int_V^0 (\Psi_\lambda \Phi_{\lambda,y})dxdyv_\beta + \int_V^0 (\Psi_\lambda)dxdy \right] = 0, \tag{16}$$

where, if $\int_V^0 (\Psi_\lambda \Phi_{\beta,x})dxdy = H_{\lambda\beta}^x$, $\int_V^0 (\Psi_\lambda \Phi_{\beta,y})dxdy = H_{\lambda\beta}^y$, and $\int_V^0 (\Psi_\lambda)dxdy = I_\lambda$ is, it is denoted as the following:

$$H_{\lambda,\beta}^x u_\beta + H_{\lambda,\beta}^y v_\beta + I_\lambda = 0, \tag{17}$$

$$u_\alpha^* [S_{\alpha\beta}^{xx} u_\beta + (S_{\alpha\beta}^{xy} - T_{\alpha\beta}^{yx})v_\beta + H_{\lambda\alpha}^x P_\lambda] = 0, \tag{18}$$

$$v_\alpha^* [(S_{\alpha\beta}^{yx} - T_{\alpha\beta}^{xy})u_\beta + S_{\alpha\beta}^{yy} v_\beta - H_{\lambda\alpha}^y P_\lambda] = 0. \tag{19}$$

Separated continuity equation (17) and equations of motion (18) and (19) can be denoted as matrix like below:

$$\begin{vmatrix} S_\alpha^{xx} & (S_{\alpha\beta}^{xy} - T_{\alpha\beta}^{yx}) & -H_{\lambda\alpha}^x & 0 \\ (S_{\alpha\beta}^{yx} - T_{\alpha\beta}^{xy}) & S_{\alpha\beta}^{yy} & -H_{\lambda\alpha}^y & 0 \\ H_{\lambda\beta}^x & H_{\lambda\beta}^y & 0 & I_\lambda \end{vmatrix} \begin{vmatrix} u_\beta \\ v_\beta \\ P_\lambda \\ 1 \end{vmatrix} = \begin{vmatrix} 0 \\ 0 \\ 0 \end{vmatrix}. \tag{20}$$

Equation (20) is derived for each finite element in the flow field and merged to obtain the finite element equation for the whole system. By substituting boundary condition to the finite element equation for the system, the corresponding flow rate and pressure can be derived.

3. **Finite Element Calculation Procedure**. In this study, slip parameter is applied to commercial GFRP composite and pre-preg intercrossed GFRP for evaluating the corresponding flow analysis theory and experimental results. The coordinate system used in governing equation is shown in Fig. 1. Governing equation with compression ratio shown in Fig. 1 is denoted as below:

$$-p_{,i}^* + \mu v_{i,jj} - 2\left(\frac{K_H}{h}\right)v_i = 0, \tag{21}$$

$$v_{i,i} + \frac{\dot{h}}{h} = 0, \tag{22}$$

where p is pressure and μ is the viscosity of material (μ is assumed to be same as μ), K_H is fluid friction coefficient, v is flow rate, and h is the thickness of the material. Equations (21) and (22) is converted to dimensionless as follows:

$$-p^*_{,i} + \frac{1}{2}\alpha v^*_{i,jj} - v^*_i = 0, \tag{23}$$

$$v^*_{i,i} + 1 = 0, \tag{24}$$

where $p^* = -p\left(\frac{2K_H \dot{h} L^2}{h^2}\right)^{-1}$, $v^*_i = \frac{dx^*_i}{dt^*}$, $x^*_i = \frac{x_i}{L}$, $t^* = \log\frac{h_0}{h}$, h_0 is initial thickness of material, and L is a characteristic length.

To verify the flow model, material acquires a square shape, and each element uses trigonal 2-dimensional one. Figure 2 shows the mesh for finite element analysis including initial element and joint. Virtual fiber is aligned in x and y direction with same spacing (81 for x direction and 81 for y direction). Using finite element method, flow rate, pressure, and the gradient is derived.

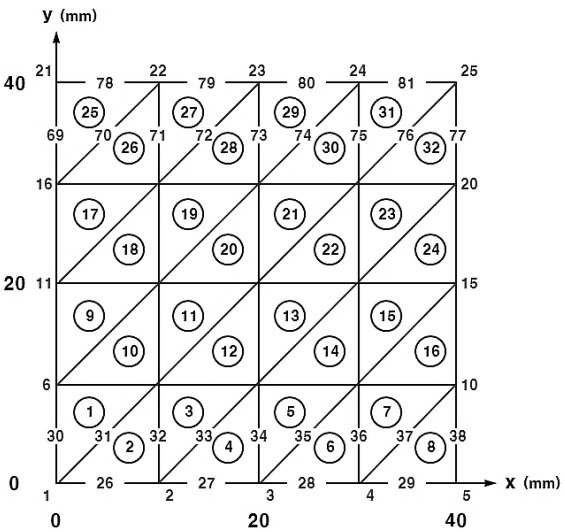

Fig. 2. Initial element, node, and mesh of FEM.

That is, joint for trigonal element and displacement of fiber is determined according to the previous calculation. On the next step, the coordinate of trigonal element and location of fiber is confirmed. Analysis target (shape of material) is set to square (80×80×3.8 mm). The number of joints is 25, and number of the elements (triangles) is 32. Target has a symmetry to x- and y-axis, and 1/4 will be used for analysis.

To obtain the finite element equation, the Galerkin method is applied. At the given time, Eqs. (23) and (24) is put together to resolve dimensionless value, v^*_x, v^*_y, and p. From v^*_x, v^*_y flow rate in x and y direction, v_x, v_y is derived. By multiplying time segment and v_x, v_y (if compression speed is 7.5 mm/s, 0.02 s), moving the displacement of each joint can be determined. From the previous coordinate for joint, the next coordinate can be derived. Until moulding is finished, above steps are repeated. That is, Eqs. (7), (8), and (9) is put together at the given time to resolve dimensionless $\bar{u}$, $\bar{v}$, and $\bar{p}$ and from $\bar{u}$, $\bar{v}$ flow rate in x, y direction, u and v [Eq. (10)] is obtained.

Flow chart for FEM methodology is given in Fig. 3. The parameter for slip parameter (α) is selected, which can influence the flow of material significantly.

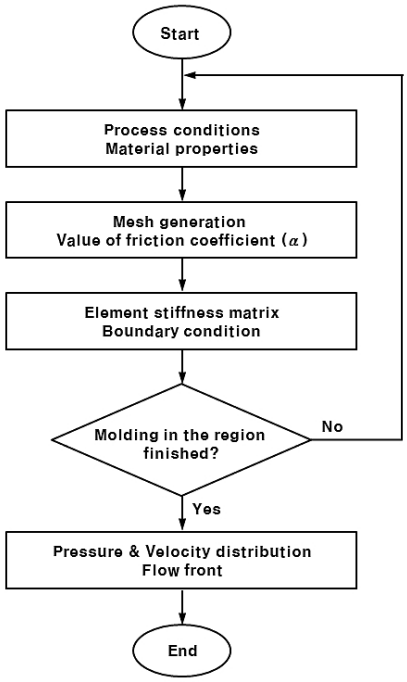

Fig. 3. Flow chart of program for analysis.

4. **Results and Discussion**. After cutting out commercially available GFRP composite into the square, it is put into hot compression flow moulding with the press. The corresponding flow analysis using FEM is compared with experimental results.

Figure 4 shows the shape of the test specimen (flow front) according to slip parameter of the interface (α). According to the figure, if $\alpha = 0$, the material is not slipped at the interface. For the shape, it tends to flow in the circular form. If slip parameter (α) is getting bigger, namely infinite, flow front can maintain initial shape.

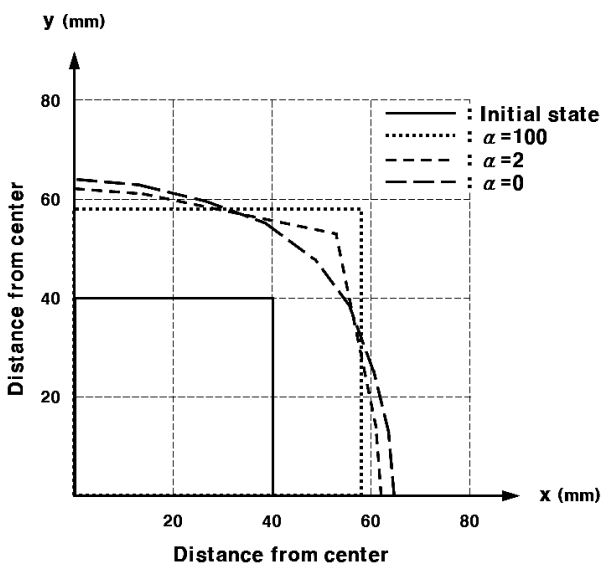

Fig. 4. Change in flow front according to α.

Figure 5 shows theoretical flow analysis results and experimental one for the previous GFRP composite with 40 wt.% fiber content ratio. In this case, slip parameter ($\alpha = 0.2$) is applied to the square shape. If fiber content ratio is 40 wt.%, 0.44 and 0.68 of compression ratio (R_{cr}) shows the good correspondence between flow analysis and experimental results.

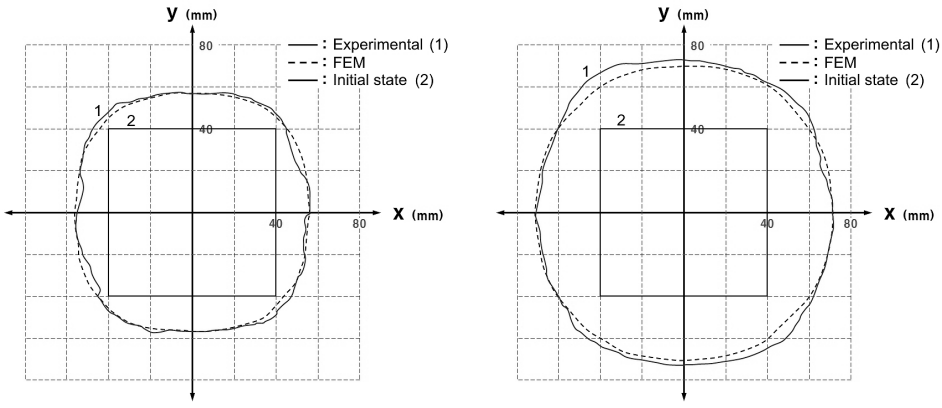

Fig. 5. Experimental and FEM shapes of initial state on GFRP (40 wt.%): (a) compression ratio $R_{cr} = 0.44$; (b) compression ratio $R_{cr} = 0.68$.

Figure 6 shows theoretical flow analysis results and experimental one for pre-preg intercrossed GFRP composite with 40 wt.% fiber content ratio. Pre-preg is made of plain weaving and stacked over. Due to tangling between fibers, the material cannot be slipped. $\alpha = 100$ of slip parameter is applied correspondingly. x:y = 1:1 and x:y = 2:1 of plain weaving shows the matching results between flow analysis and actual experimental results. Plain weaved GFRP pre-preg no happen separation of matrix and resin and fiber orientation. Therefore, matrix and reinforcement is well formed.

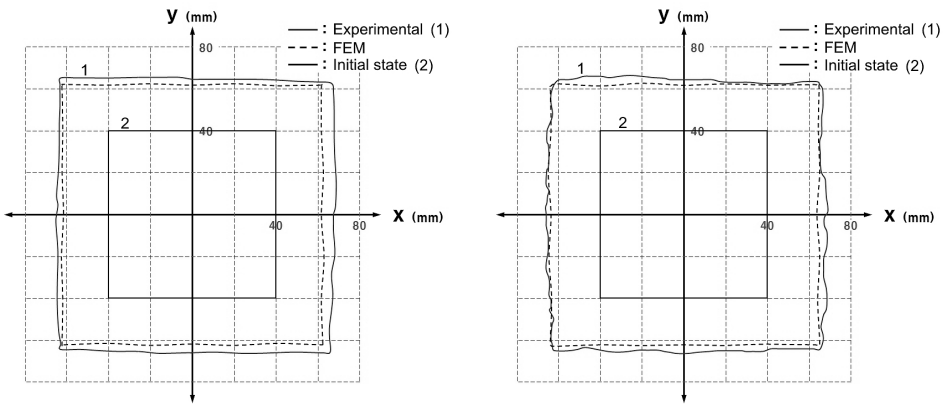

Fig. 6. Experimental and FEM shapes of initial state on 0/90° fabric GFRP (40 wt.%, $R_{cr} = 0.55$): (a) x:y = 1:1; (b) x:y = 2:1.

Conclusions. GFRP pre-preg is prepared, and it is used to manufacture intercrossed GFRP composites. Manufactured composites are under hot compression flow moulding, and the following results are achieved. Pre-preg intercrossed GFRP composite is made of stacking plain weaved pre-preg, and material cannot be slipped by the entanglement between fibers.

Based on the assumption of the significant influence of friction, $\alpha = 100$ of slip parameter is used in FEM flow analysis according to the Galerkin method, which is well matched to experimental results. Therefore, various intercrossing methods, such as twill, silk weaving, textus, Mock Leno, etc. other than plain weaving, can be applied to prepare GFRP composite. Structural stability, fiber deformation, and mechanical strength of these materials should be evaluated and built the database. Using this database, these materials can be widely used in industry, such as tank or container in chemical industry, ship body of small ship and yacht, structural member of automobile, pipelines, and aerospace industries, etc.

Acknowledgments. This study was supported by research fund from Chosun University (2015).

1. J. W. Kim, H. S. Kim, and D. G. Lee, "Effect of molding condition on waviness profile of GFRP composites in compression molding," *Acta Physica Polonica A*, **123**, 337–340 (2013).
2. C. Meola and G. M. Carlomagno, "Impact damage in GFRP: New insights with infrared thermography," *Composites Part A: Appl. Sci. Manuf*., **41**, 1839–1847 (2010).
3. H. Yan, J. T. Zhang, and P. C. Zhai, "Discrete element modelling on creep behaviour of PI/SiO_2 composite," *Mater. Res. Innov*., **18**, Suppl. 4, S4-1057–S4-1061 (2014).
4. C. Chen, Y. Qian, A. Wang, et al., "Optimised design of structure for orthotropic piezoelectric fibre composite materials based on Ansys," *Mater. Res. Innov*., **18**, Issue S2, S2-136–S2-139 (2014).
5. O. Kumbuloglu, L. V. J. Lassila, M. Turkun, and P. K. Vallittu, "Effect of various disinfection methods on bonding strength of glassfibre post to root canal dentine," *Mater. Res. Innov.*, **16**, Issue 2, 79–83 (2012).
6. T. T. Do and D. J. Lee, "Analysis of tensile properties for composites with wrinkled fabric," *J. Mech. Sci. Technol.*, **24**, No. 2, 471–479 (2010).
7. J. W. Kim, H. S. Kim, and D. G. Lee, "Study on fiber orientation of weld line parts during injection molding of fiber reinforced plastic by image processing," *Mater. Res. Innov.*, **15**, Issue S1, S1-303–S1-306 (2011).
8. M. S. Sureshkumar, D. Lakshmanan, and A. Murugarajan, "Experimental investigation and mathematical modelling of drilling on GFRPcomposites," *Mater. Res. Innov.*, **18**, Issue S1, S1-94–S1-97 (2014).
9. J. Ryu, Y. K. Ju, S. W. Yoon, and S. D. Kim, "Bending capacities of glass fiber reinforced plastic composite slab," *Mater. Res. Innov.*, **17**, Suppl. 2, S12–S18 (2013).
10. J. F. Dong, P. Jia, S. C. Yuan, and Q. Y. Wang, "Compressive behaviours of square timber columns reinforced by partial wrapping of FRP sheets," *Mater. Res. Innov.*, **19**, Issue S1, S1-465–S1-468 (2015).
11. D. G. Lee and J. W. Kim, "Effect of mould temperature on separation and orientation during compression moulding of fibre reinforced composites," *Mater. Res. Innov*., **18**, Issue S2, S2-382–S2-386 (2014).
12. J. W. Kim, H. S. Kim, and D. G. Lee, "Manufacturing and characterization of glass fiber/polypropylene prepreg for automotive bumper beam," *J. Comput. Theor. Nanosci.*, **12**, No. 5, 842–846 (2015).
13. D. G. Lee and J. W. Kim, "Study on the measurement of fiber orientation during press molding of long fiber-reinforced thermoplastic composites using counting method," *J. Comput. Theor. Nanosci*., **12**, No. 5, 875–879 (2015).
14. H. Yu, S. Chen, Y. Jiang, et al., "Modelling thermal damage mechanism of dam in extremely frigid area by FEM," *Mater. Res. Innov.*, **18**, Issue S2, S2-978–S2-981 (2014).

Received 03. 08. 2015